

Mesoscale activity in the North Sea as seen in ensemble simulations

Arne Melsom

Norwegian Meteorological Institute, P.O. Box 43 Blindern, 0313 Oslo, Norway

Abstract A set of two simulation ensembles of the ocean circulation in the North Sea, the Skagerrak and bordering seas has been run for the ten year period that started in January 1992. The ensembles differed only in the horizontal grid resolution. The main purposes of this investigation are (1) to quantify the variability that can be expected in multi-year simulations due to noise-like perturbations in the initial fields, and (2) to examine the robustness of model results for mesoscale features that form on the front between the Norwegian Coastal Current and water masses that are of an Atlantic Ocean origin. It is shown that the model resolution has a substantial impact on the ensemble variability, and that the role of small perturbations become more significant as the grid mesh is refined. Nevertheless, it is demonstrated that in a region to the west of the southern tip of Norway, eddies are occasionally found in the same positions at the same time in the results from all members of the ensembles. This is particularly the case in the aftermath of outbreak events of low salinity water masses from the Skagerrak into the North Sea.

Key words ensembles – mesoscale – eddies – North Sea

1 Introduction

The current along the coast of southern Norway is the wedge-shaped Norwegian Coastal Current (NCC). This current carries an average of $0.25\text{-}1\cdot 10^6 \text{ m}^3/\text{s} = 0.25\text{-}1 \text{ Sv}$ (Sverdrup) from the Skagerrak into the North Sea, and further north into the Norwegian Sea (*e.g.* Gammelsrød and Hackett [10]). From both observations and model studies we know that mesoscale features like meanders and eddies are abundant on the front between the NCC and the saltier Atlantic Water to the west, see *e.g.* Sætre [21] and Røed and Fossum [19].

The variability of the NCC on a time scale of days is dominated by the influence of atmospheric forcing. It

has been suggested that extreme currents in the North Sea, with speeds exceeding 1 m/s, are related to outbreak events of water masses with relatively low salinities from the Skagerrak. Such events occur when the wind relaxes or changes direction after a period when moderate or strong south to southwesterly winds have piled up water in the Skagerrak (Aure and Sætre [1]).

Furnes et al. [9] discuss the relation between these wind events and the intensity of the mesoscale circulation in the aftermath of an outbreak of low salinity water from the Skagerrak. If a relation exists, then the intensity on the mesoscale is linked to the wind history. Further, it has been suggested that the position of ocean eddies in parts of this region could be linked to bottom topography features where vortex stretching and squeezing occur (Røed and Fossum [19]). Then, it is conceivable that it is possible to forecast ocean eddies in this region even when the initial state is poorly known.

In the light of the literature on these topics, the present study aims at answering the following questions: To what degree does a hindcast study of the circulation of the Skagerrak and the North Sea depend on initial conditions that are produced by climatological atmospheric forcing fields, and how much of the variability can be ascribed to nonlinear flow instabilities? Further, can eddies that form on the front between the NCC and saltier Atlantic Water be “deterministic” in the sense that they can be forecasted when the atmospheric forcing fields are known, but initial conditions are not?

In order to answer these questions, we have conducted two suites of ensemble simulations. The analysis will mostly consider properties of the simulation results that represent the statistics of the ensembles. However, due to the intermittent character of the episodes that have been reported by Aure and Sætre [1] and Furnes et al. [9] we have also analyzed a pair of selected events.

In a hindcast simulation of the ocean circulation, such as the one carried out in this investigation, there are two strategies for ensemble simulations that can be em-

ployed while observations are more or less ignored. One of these strategies involves production of initial fields that provide a description of the historic ocean circulation variability. In a study of the global ocean circulation, initial fields would typically be selected from different states of the meridional overturning circulation. Such a strategy was adopted by Bentsen et al. [2] in their study of multi-annual to decadal scale variability of the Atlantic meridional overturning circulation. In a regional study, such a strategy could be pursued by spinning up the model to initial states by applying atmospheric forcing that corresponds to various atmospheric circulation patterns.

The other strategy is to generate initial fields whose only differences are of a “noise-like” nature. Then, the variations between ensemble members will be a measure of how results are affected by nonlinear processes that give rise to error growth. In the absence of observations such initial fields may be emulated by continuing a climatologically forced model spin up beyond the time when a statistical equilibrium is reached. The initial fields are then selected from subsequent “post spin up” years. This strategy was adopted by Metzger and Hurlburt [18] in their investigation of Kuroshio intrusion into the South China Sea, and by Melsom et al. [17] in their study of remote oceanic forcing in the Gulf of Alaska. In the present study, the latter strategy for ensemble simulations will be adopted.

An outline of this article is as follows: In section 2 the ocean circulation model is presented and its present configuration is described. The model validation in section 3 reveals that the NCC in the model is too wide and slightly lacking in buoyancy, and the dynamics responsible for these deficiencies are examined. Then, relations between the ensemble size and convergence are discussed in section 4. Next, in section 5 we demonstrate that the model resolution has a substantial impact on the relative roles of atmospheric forcing and flow instabilities with respect to the variability of the ensemble. Nevertheless, based on the present suites of simulations we find in section 6 that “deterministic” eddies evolve to the west of the southern tip of Norway, particularly in the aftermath of Skagerrak outbreak events. Finally, we provide additional interpretations of some results in section 7.

2 The ocean circulation experiments

2.1 The ocean model

The present study has been conducted using the Hybrid Coordinate Ocean Model (HYCOM). HYCOM is a generalized-coordinate mass conserving ocean circulation model that has evolved from the Miami Isopycnic Coordinate Ocean Model (MICOM) (Bleck et al. [4], and references therein). Details about HYCOM has been described by Bleck [3], and documentation and additional information about HYCOM can be found on-line

at <http://hycom.rsmas.miami.edu>. HYCOM version 2.1 was available for the present study.

The vertical coordinate in HYCOM is initially specified by target densities, and when the requested specification of layers can be met, the model layers are isopycnic. As a result, the isopycnic layers normally span the water column beneath the mixed layer in the deep, stratified ocean. There is a smooth transition to terrain-following coordinates in shallow coastal regions, and to z -level coordinates in the mixed layer and/or unstratified seas. The hybrid coordinate algorithm has been described in detail by Bleck [3], and various specifications of the vertical coordinate have been described and tested for an Atlantic Ocean configuration by Chassignet et al. [6].

The HYCOM user may select one of several vertical mixing parameterizations. A detailed discussion of how HYCOM performs when five different mixed layer models are used, is given by Halliwell [11]. For this study, the K-Profile Parameterization (KPP) closure scheme (Large et al. [15]) was chosen. This is a semi-implicit scheme which includes prognostic equations for diffusivity and viscosity. There is a smooth transition from the diffusivity and viscosity profiles in the mixed layer to the diapycnal diffusivities and viscosities beneath the mixed layer. The KPP scheme includes parameterization of wind-induced mixing and surface buoyancy fluxes in the mixed layer, while beneath, the contribution from internal wave breaking, shear instability and double diffusion are taken into account.

2.2 The model configuration

Mesoscale features that are associated with flow instabilities are pivotal in this study. These features arise due to baroclinic instability, when potential energy is converted to kinetic energy. The main source of potential energy in the North Sea is the buoyant NCC, and mesoscale features in the North Sea mainly form on the front between the NCC and the saltier water masses further off shore.

In this context it is crucial to resolve scales at which features that are associated with non-linear flow instabilities, occur. Further, in order to capture a number of Skagerrak outbreak events, as well as seasonal and year to year variability, a multi-year simulation of the regional ocean circulation was conducted. Together with the finite amount of available computer resources, these requirements made it necessary to configure the model with a coarse vertical resolution, and a modest number of ensemble members.

The model domain, which is displayed in Figure 1, consists of the North Sea, the Skagerrak and the Kattegat, and the southern part of the Norwegian Sea. The model was configured on a spherical grid, using a set of two different horizontal resolutions. In the coarse resolution experiment (CRE) a uniform resolution of 0.16° longitude by 0.08° latitude was specified. The fine resolution

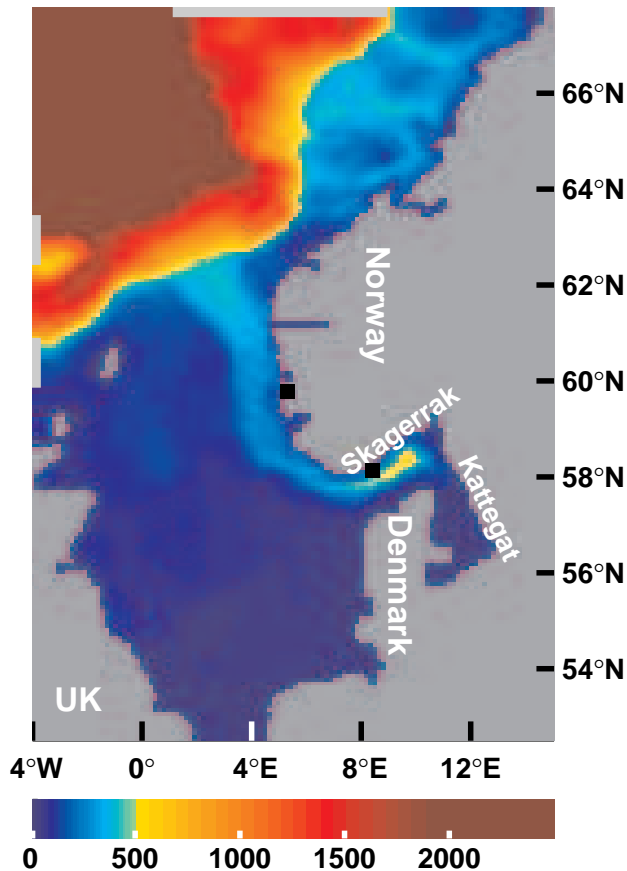


Fig. 1 Model domain and the bottom topography in meters. The color coding is given by the color bar at the bottom. The land mask is given by the dark gray regions. Light gray lines along the western and northern boundaries indicate the position of ports, see section 2.2 for details. This depiction corresponds to the coarse resolution experiment (CRE). Black markers on the coast of southern Norway indicate the positions of the cities of Bergen (in the west) and Lillesand (in the south).

experiment (FRE) was conducted on a grid resolution of 0.08° longitude by 0.04° latitude. At the latitudes of the North Sea, the horizontal resolutions in the CRE and the FRE are about 9 km and 4.5 km, respectively.

The simulations were conducted using seven hybrid layers. Their respective target densities were set to $\sigma_t = 26.0, 26.4, 26.8, 27.2, 27.5, 27.8, 28.1 \text{ kg/m}^{-3}$. This configuration led to a z -layer of 3 m depth as layer 1. The thickness of layer 2 was variable, with values around 10 m in the North Sea. The thickness of the deep layers was even more variable, and the largest values in the North Sea were obtained in the Norwegian Trench in layer 3 – 6 with layer thicknesses of about 50 m. The southern Norwegian Sea, which is poorly resolved in the vertical, was included in order to allow for wind induced variations in the transport of salty Atlantic Water into the northern North Sea. The maximum depth was set to 2500 m, in order to reduce the constraint of the integration time

step. (The actual maximum depth in the present region is around 4000 m.)

The bottom stress is parameterized by a bottom drag that is proportional to the square of the velocity. Otherwise, the present implementation of the KPP scheme in HYCOM does not include a parameterization of mixing in the bottom boundary layer.

The lateral boundaries of the domain were set to 4°W in the west, $15^\circ 02' \text{ E}$ in the east, $52^\circ 30' \text{ N}$ in the south, and $67^\circ 47' \text{ N}$ in the north. This corresponds to resolutions of 121 by 193 grid nodes and 242 by 385 grid nodes in the CRE and the FRE, respectively. Along open lateral boundaries, Newtonian relaxation was applied in sponge zones that extended six and eight grids into the CRE and FRE domains, respectively. In these zones, the relaxation time scale was set as a linear function of distance from the boundary, varying from 30 days at the boundary to 180 days at the innermost grids of the sponge zones. Also, the sea surface temperature was nudged toward the climatological values by a bulk formulation in which the e-folding time is proportional to the mixed layer depth in the model. The monthly climatology of hydrography from the Institute for Marine Research and the Norwegian Meteorological Institute (Engedahl et al. [7]; Engedahl et al. [8]) was applied for these purposes. Relaxation of the sea surface salinity was not applied.

In order to include effects of the brackish water masses in the Baltic Straits, we defined a sponge zone that covers the southern part of the Kattegat. The sponge zone was set to extend from top to bottom in the water column, eleven grids and seventeen grids into the Kattegat in the CRE and the FRE, respectively. The relaxation time scale in the sponge zone was set to values between 10 and 40 days, with the most gentle relaxation in the north. The same monthly climatology of hydrography as above was applied for this purpose.

Moreover, to account for the flow of salty waters by the Norwegian Atlantic Current in the northern region, barotropic flow normal to the boundary was specified at three model ports, using the well-posed boundary conditions by Browning and Kreiss [5]. At two ports along the western boundary, the westward barotropic flow into the model domain was set to 0.4 Sv, equally partitioned (0.2 Sv at each port). Further, at a port along the northern boundary the northward barotropic flow out of the domain was set to 0.4 Sv. The specification of the outflow at the northern boundary included an intensification over the continental slope. The ports are indicated by light gray lines in Figure 1. The size of the domain, the choice of applying a sponge zone in the Kattegat, and the magnitude of the barotropic flow of salty waters, were made based on results from a set of exploratory simulations with climatological atmospheric forcing and model configurations similar to the CRE.

The HYCOM simulations were performed with surface fluxes from the National Centers for Environmen-

tal Prediction (NCEP)/National Center for Atmospheric Research (NCAR) reanalysis data set (Kalnay et al. [14]). The model was initialized according to the prognostic monthly ocean climatology due to Engedahl et al. [7], and spun up to a statistical equilibrium with a climatology of monthly mean surface fluxes. The monthly surface flux climatology was calculated from NCEP/NCAR reanalysis data for the period 1985 – 1991. Later, the simulations were continued using synoptic (6 hourly) surface fluxes for the period 1992 – 2001. Surface fluxes of air temperature at 2 m, net total radiation, net long wave radiation, water vapor mixing ratio, wind speed, and momentum flux components toward east and north were used to force the simulations. Depending on water clarity, the short wave radiation was allowed to penetrate beyond the upper model layer, due to a parameterization that is based on the water type definitions by Jerlov [13].

Discharges from 41 rivers were included as precipitation at the appropriate coastal grids, using constant climatological values. Elsewhere, there was no net fresh-water flux across the ocean’s surface.

Although tides are of a moderate to large magnitude in the North Sea, tidal forcing was not applied in this study. The main reason for this choice is that tides have little or no impact on neither the role of flow instabilities, nor the Skagerrak outbreak events.

The simulations were performed with salinity as the prognostic ocean state variable. In non-isopycnic layers, the density was also treated as a prognostic variable, and the temperature was diagnosed from the equation of state. The experiment set up described here was based entirely on the standard set of options in HYCOM.

Initial fields for the various members of the ensembles were taken from results for January from simulations that were forced with monthly atmospheric climatologies. The CRE reached a state of statistical equilibrium after 15 years, and the initial fields for the eight members of the CRE ensemble were taken from the results for January from years 16 – 23. The results for January from year 23 were then interpolated to the FRE grid, and a statistical equilibrium for the FRE was reached after an additional 12 years of simulation. This simulation was then extended, and the initial fields for the FRE ensemble members were taken from the results for January from years 35 – 42. The only difference in the configuration for the CRE ensemble members are their initial fields. The same statement is true for the FRE ensemble.

2.3 Model results

Model results were stored every 48 hours, at all horizontal grids and for all layers, as specified in section 2.2. With the exception of the viscosity and diffusion coefficients, results for all prognostic variables were available for this study (salinity, density, velocity, layer thickness,

sea surface height (SSH), and the Montgomery potential). By inspecting the results from the North Sea and the Skagerrak we found that this output frequency yields a fair representation of the depth dependent (“baroclinic”) variables, since there are typically 5 values or more between the local extrema in time series from one grid node.

Results from synoptically forced simulations may be sensitive to processes such as inertial oscillations if the vertical resolution is too coarse. Such contamination was not found in the time series of the baroclinic variables from the North Sea and the Skagerrak, neither in frontal regions nor elsewhere. However, rapid fluctuations were occasionally seen in the time series from the southern Norwegian Sea.

On the other hand, the depth integrated (“barotropic”) variables are not resolved in time. Hence, the analysis in this study will be restricted to results for the baroclinic variables. In an examination of results from the CRE, Melsom [16] found that time series of model results contained trends in the first 3 – 4 years of the simulation period, due to the transition from climatological to synoptic atmospheric forcing. Hence, the analysis of the model results will be restricted to the period November 1996 – October 2001.

In this study, we will examine results for two quantities that are derived from the prognostic variables. First, we define the baroclinic sea surface height (bSSH) as

$$h = \frac{1}{g} \sum_{l=1}^L \frac{\Delta p_l}{\rho_l} - H_0 \quad (1)$$

where ρ_l is the density of layer l , and $\Delta p_l = p_{l+1} - p_l$ is the pressure difference from the bottom to the top of layer l (p_l is the pressure at the top of layer l). Furthermore, g is acceleration due to gravity, and H_0 is a reference depth. This quantity expresses the contribution to SSH from changes in the vertical density profile, and it is a vertically integrated property. Moreover, since it is derived entirely from baroclinic variables the frequency of available results is acceptable. Since the bottom pressure p_{L+1} in Equation (1) is time invariant in HYCOM, variations in the baroclinic sea surface height are equivalent to the local dynamic height anomalies.

Second, the relative vorticity is defined by

$$\zeta = \frac{\partial v}{\partial x} - \frac{\partial u}{\partial y} \quad (2)$$

where u and v are the velocity components in the x and y directions, respectively, evaluated at some depth. The depth integrated velocity is a substantial, rapidly varying part of the total velocity in a wind infested high-latitude shallow sea like the North Sea. Hence, we will restrict the analysis of the relative vorticity to results for the well resolved depth dependent (baroclinic) part of the velocity field.

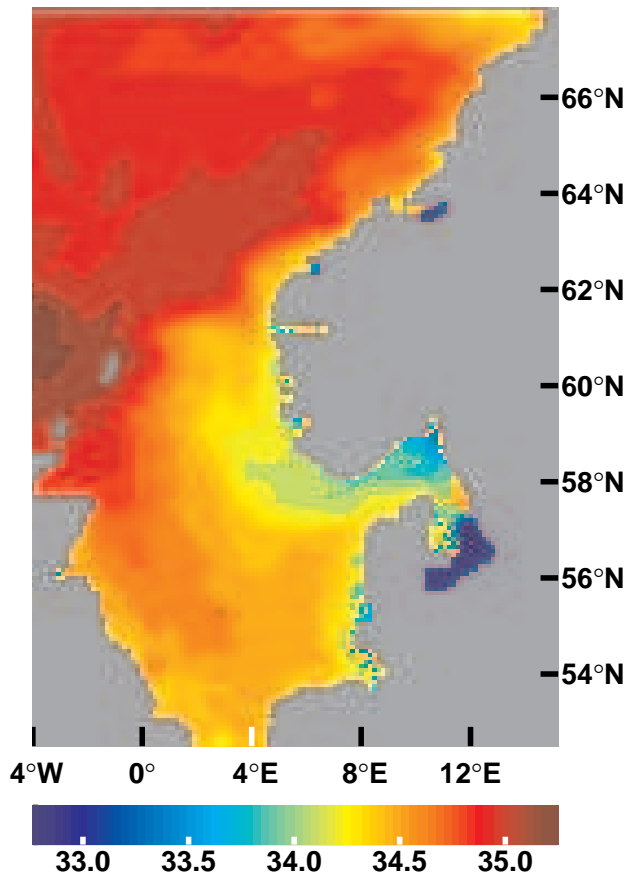


Fig. 2 Mean salinity for March at a depth of 30 m, based on the model simulation for 1997 – 2001. The color coding is given by the bar in the lower panel with values in PSU units. This depiction shows results from ensemble member *no.* 4 in the CRE.

Much of the presentation of results for the depth-dependent variables will be given for specific depths. For this purpose results were extracted at the requested depths, rather than applying vertical interpolation between the center levels of the layers.

3 Model validation

The observational data that are available for this investigation are the monthly ocean climatology from the Institute for Marine Research and the Norwegian Meteorological Institute (IMR/met.no) (Engedahl et al. [8]). The hydrographic data were derived from *in situ* observations, and they were gridded with a horizontal resolution of 20 km and at standard observational depths in the vertical. Further, Engedahl et al. [7] performed a diagnostic model simulation using the IMR/met.no hydrographic data. For each month of the year, their diagnostic simulation was extended by 30 day prognostic simulations, in order to arrive at a more dynamically consistent flow field. Note that this prognostic archive

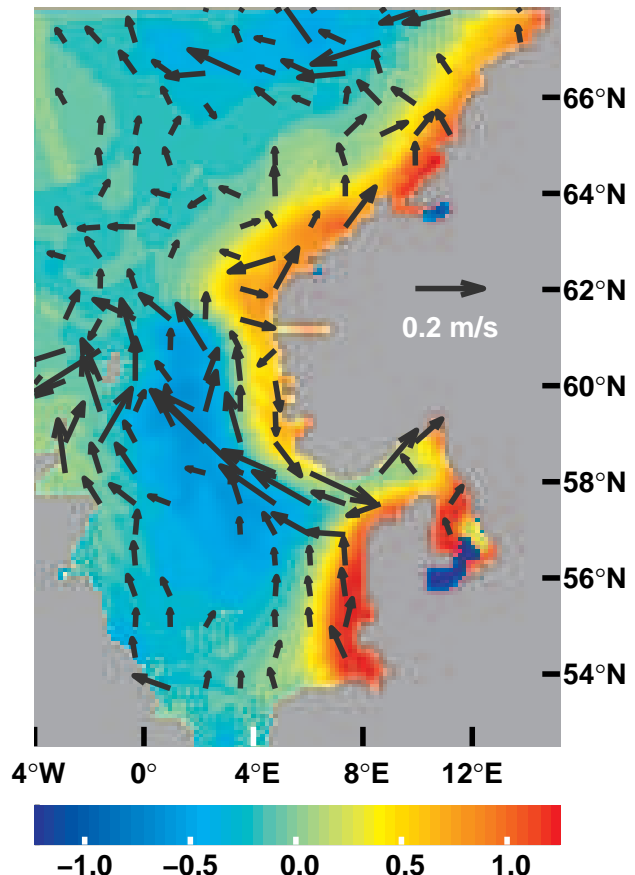


Fig. 3 Differences in simulated and climatological salinities and velocities for March at a depth of 30 m. The color coding is given by the color bar in the lower panel with values in PSU units, and a caption arrow that corresponds to a velocity difference of 0.2 m/s is displayed over southern Norway. Positive salinity anomalies correspond to higher values in the present study when compared to the IMR/met.no climatology. Vectorial differences were computed analogously, *i.e.*, by subtracting the IMR/met.no velocities from those obtained in this study. Vectors are drawn for every eighth grid node in the x - and y -direction of the CRE (member *no.* 4), but vectors corresponding to a speed difference less than 0.05 m/s have been discarded.

differs from the prognostic archive that was documented by Engedahl et al. [8].

Additionally, monthly data of *in situ* observations of hydrography from the Hirtshals – Torungen transect across the Skagerrak from northern Jutland in Denmark and northeastward to Norway, were available for this study. These data were supplied by the IMR.

The model salinity climatology for March at a depth of 30 m in the present study is displayed in Figure 2. Along the coast of southern Norway, we observe features that are typical for the Norwegian Coastal Current: The NCC is characterized by water masses with relatively low salinities, primarily of a Baltic Sea origin. As these water masses flow along the coast of southern Norway from the Skagerrak into the North Sea and further into

the Norwegian Sea, they are mixed with saltier water masses of an Atlantic Ocean origin. However, the results in Figure 2 reveal that the modeled coastal current is too wide. As a consequence, salinities become too high near the Norwegian coast, and too fresh in the remaining eastern North Sea, and the Atlantic Water are displaced westward. The high mixing rate of Atlantic Water into the NCC leads to higher salinity values in the model results than in the IMR/met.no climatology.

The differences in March between salinities and velocities in model results and the IMR/met.no prognostic archive are displayed in Figure 3. Here, values from the IMR/met.no archive were subtracted from the corresponding model results. The depiction in Figure 3 can thus be interpreted as transport of salinity anomalies in the model results. The wide coastal current in the model can be seen as a fresh anomaly that is transported north-westward, west of the Norwegian trench in the North Sea. We also observe that a salt anomaly is transported from the German bight along the west coast of Jutland. This relatively salty water apparently affects the salinities in the northern Kattegat. In this way, the NCC becomes too salty in the model, and the front between the NCC and the Atlantic water is too weak. Hence, the wide NCC in the model reflects a buoyancy that is lower than in the IMR/met.no climatology.

The above discussions of results displayed by Figures 2 and 3 that are based on the March climatologies, are representative for the upper 50 m, and for all months of the year.

In order to examine variability, model results for hydrography were compared with observations from the Hirtshals – Torungen transect, and with the IMR/met.no monthly climatology. For this purpose, model results were extracted at depths and dates that corresponded to the transect data. We found that salinities in both the transect data and in the model results were higher than in the climatology. At 30 m, the largest offsets were found for the transect data near the west coast of Jutland, where the mean differences between the 1997 – 2001 data and climatology were as large as 0.75 – 1 PSU. At levels above 30 m, the largest differences are found for the offsets of model results from climatology, again predominantly along the Danish coast.

Correlations between the transect data and the corresponding model results are very low (0.25 or less), indicating that the temporal variability is not realistic in the model. In this context, it should be mentioned that overall mean values were used for the freshwater runoff data, rather than monthly means or actual data with a realistic temporal dependence.

Observations from the Hirtshals – Torungen transect are included in the IMR/met.no observational climatology. However, this climatology was constructed in 1996, so the presently examined transect data are independent of the climatology.

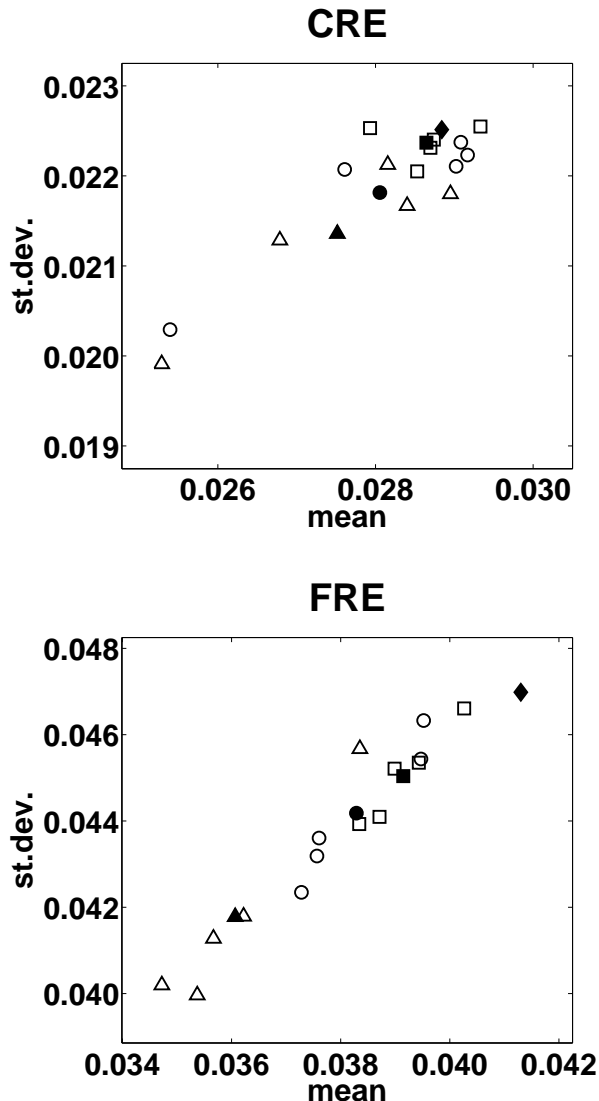


Fig. 4 Convergence of results for r_h^{nd} . Displayed in the top and bottom panels are spatial mean values and spatial variances (nondimensional) from various samples of the eight member CRE and FRE ensembles, respectively. The following symbols were used: 8 members (\diamond); 7 members (\square); 6 members (\circ); 5 members (\triangle). Ensembles with 5, 6, and 7 members were each constructed from five different sub-samples of the full ensembles. An open symbol shows results for a sub-sample, while filled symbols correspond to the averages for the various ensemble sizes. These results are for the region south of $61^\circ 30' N$. See the text for details.

4 Ensemble size and convergence

A widely used method to assess the performance of an ensemble in the context of weather forecasting is to construct rank histograms where model values are compared with observations. If there is no bias in the model results, and if the ensemble spread is a proper measure of variability, the rank histogram becomes flat for a reliable ensemble (Hamill [12]).

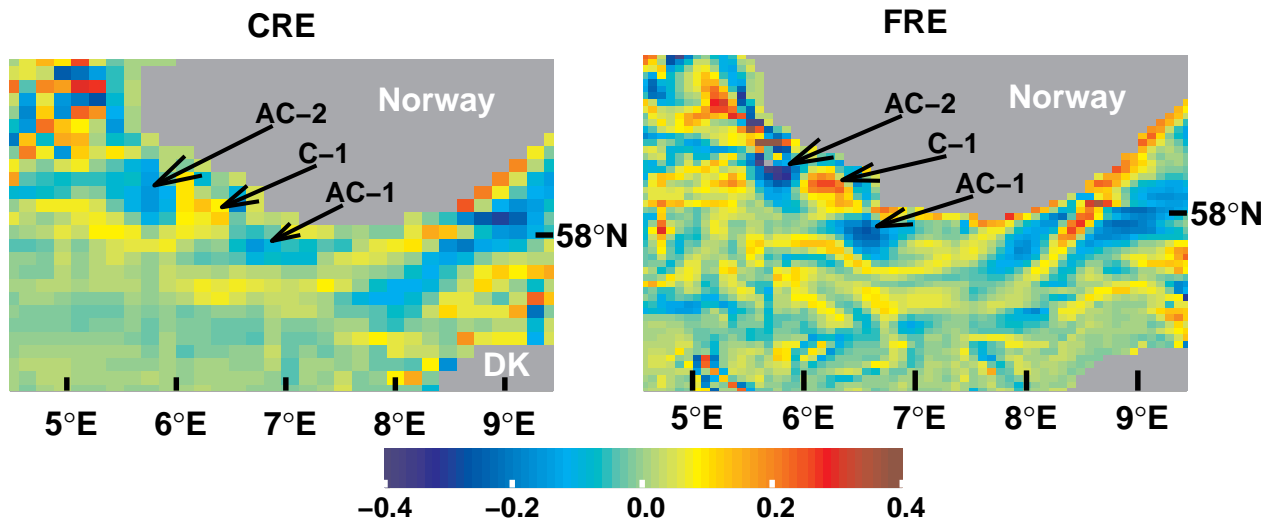


Fig. 5 Model results for relative vorticity off the south coast of Norway. The relative vorticity were computed for a depth of 10 m, and displayed model results are for 25 September 2000. The vorticity values were scaled by the local Coriolis parameter. Positive and negative values correspond to cyclonic and anticyclonic circulation, respectively. Results from ensemble member *no.* 4 of the CRE and the FRE are displayed in the left and right panels, respectively. Two anti-cyclonic eddies have been labeled AC-1 and AC-2, while a cyclonic eddy in between was labeled C-1. The nondimensionalized values for vorticity is indicated by the color bar.

The method of rank histograms was applied to the salinity and temperature data from the Hirtshals – Torungen transect. From the analysis in section 3 we found that there is a significant bias in the model in this region. However, even after the bias was removed the rank histograms revealed that the variability in the model results was very low, with almost all observations being outside the range spanned by the ensemble. Hence, the present approach for model initialization leads to lower ensemble variances than in the case when the model initialization is a synthesis of observations and results from an earlier model run.

As an alternative, we assess relations between the size and convergence of the ensembles by examining properties of the fraction of nondeterministic variability of the bSSH, r_h^{nd} , see the Appendix for details on the derivation of this quantity. The mean values and standard deviations of r_h^{nd} from various CRE and FRE ensemble constructions are presented in the top and bottom panels of Figure 4, respectively. The contribution that may be linked to problems with the prescribed flows across the northern boundaries was eliminated by restricting these calculations to the region south of 61° 30'N (see the discussion on this topic in section 5). Both panels have been sized so that the length of the x and y axes correspond to 20% of the values for the full (8 member) ensembles.

Figure 4 reveals that the mean values and standard deviation of r_h^{nd} increase with finer resolution, as expected. We also note that these quantities increase as the ensemble size grows. The CRE results in the top panel indicate that the ensembles for this resolution are close to convergence with 7 – 8 members. Averages based

on FRE ensemble results for r_h^{nd} suggest that the FRE may require more than 8 members in order to converge (bottom panel). The spatial patterns of r_h^{nd} from the full ensembles will be examined in the next section.

5 Model resolution and nonlinear processes

As described in section 2.2, ensemble simulations were performed on two spherical coordinate grids, with horizontal resolutions of approximately 9 km (coarse resolution experiment, CRE) and 4.5 km (fine resolution experiment, FRE), respectively.

In the region of interest the CRE is an experiment that is eddy permitting, while the FRE is approaching a fully eddy resolving ocean circulation simulation. This is indicated by the results depicted in Figure 5, where snapshots of the relative vorticity for both resolutions are displayed, for 25 September 2000. Only a subdomain is displayed in this figure, in order to display mesoscale circulation features that are of fairly small horizontal sizes. A string of three eddies can be identified in both the CRE and the FRE, as shown by the labeled arrows in Figure 5. There are also hints of a second cyclonic eddy to the northwest of eddy AC-2, particularly in the FRE. As expected, the eddies are more intense in the FRE than in the CRE. The anticyclonic eddies are easily identified at 50 m depth in the FRE, while there is no obvious evidence of cyclonic eddies at this level (not shown).

We also note that eddies as well as other circulation features display remarkable similarities in the CRE

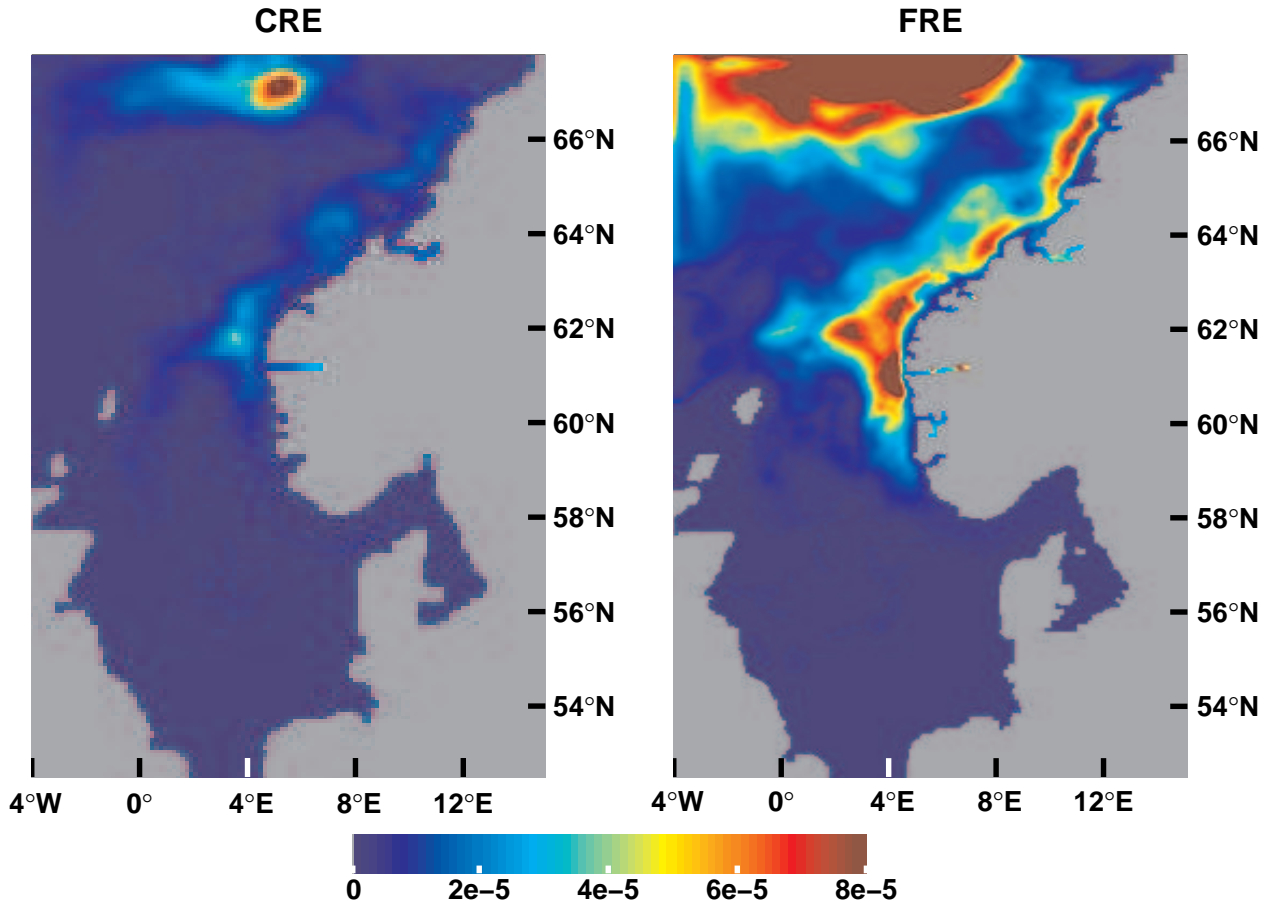


Fig. 6 Variance of baroclinic sea surface height ($\overline{\eta_s'^2}^n$) among the eight member CRE and FRE ensembles. These are the time means for the period November 1996 – October 2001 for all grid nodes after the ensemble variance has been calculated for each time step. Results from the CRE and the FRE are displayed in the left and right panels, respectively. The color coding of the variances are indicated by the bar, with values in m^2 .

and the FRE for this particular situation. Differences in amplitude aside, these features are seen to be situated at the same geographical positions. Hence, these results of coinciding eddies in space and time in the CRE and the FRE suggest that under certain circumstances, eddy generation may primarily be linked to the regional wind history, and small differences in the initial conditions may be unimportant. Moreover, the bottom topography may be the agent that determines the positions of eddy formation. Røed and Fossum [19] suggest that vortex stretching and squeezing by flow over topographic features in this region act as eddy triggers. This hypothesis of “deterministic eddies” will be investigated in the next section.

Next, we consider relations between variability in ensembles and model resolution. The properties of ensemble variability that will be considered here, are the ensemble variance and the fraction of nondeterministic variability. The mathematical definition of these quantities are given in the Appendix, where they are denoted by $\overline{\eta_s'^2}^n$ and r^{nd} , respectively. The nondeterministic variability is high wherever the ensemble variance is a rela-

tively large fraction of the total variance with respect to the daily climatology of the model results. Conversely, the nondeterministic variability is low when the ensemble variance is relatively small, *i.e.*, when the root mean square offset from the climatology can almost solely be attributed to the variability in the atmospheric forcing.

In Figure 6 the time mean of the ensemble variance $\overline{\eta_s'^2}^n$ at each grid node is displayed, based on results for bSSH from the period November 1996 – October 2001. Left and right panels display the variances for the CRE and FRE ensembles, respectively. The large values that are found in the north, where a wide outflow port was applied, may be associated with nonlinear processes that are related to the configuration of the experiment. Away from the open boundaries, we find the highest variances in the vicinity of the model’s representation of the frontal regions between the Norwegian Atlantic Current and the NCC off the northwestern coast of southern Norway. Here, relatively large horizontal gradients are seen in the salinity field that is displayed in Figure 2. The variances are significantly higher in the FRE than in the CRE. However, the geographical patterns of the variances in

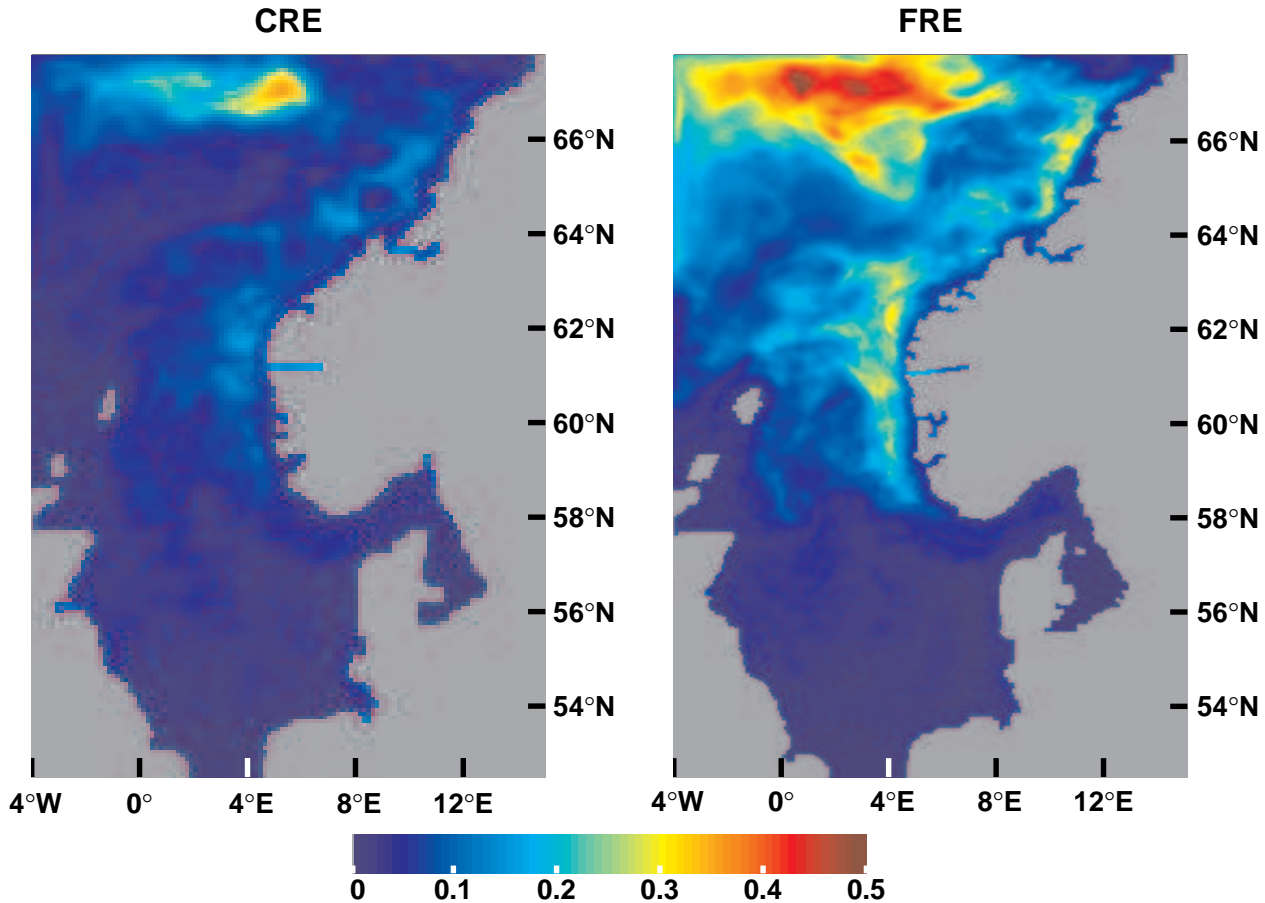


Fig. 7 Fraction of nondeterministic variability in bSSH (r_h^{nd}) from the ensemble results. These are the time means for the period November 1996 – October 2001 for all grid nodes. Results from the CRE and the FRE are displayed in the left and right panels, respectively. Nondimensional fractions are displayed by the color bar.

the CRE and FRE are similar, with magnitudes differing by about a factor of 4 (not shown).

The ensemble variance is not necessarily an adequate measure of how the model results are affected by nonlinear processes associated with flow instabilities: The ensemble variance may be high in regions where there is a large variability that can be attributed to time variations in the synoptic atmospheric forcing fields. The latter type of variability will hereafter be referred to as deterministic variability since the atmospheric forcing fields are assumed to be known *a priori* in the present context. The relative importance of nondeterministic flow instabilities and deterministic variability may thus lead to horizontal patterns that are different from those seen in Figure 6. Moreover, the differences between the CRE and the FRE may also be affected.

The fractions of nondeterministic variability of bSSH (r_h^{nd}) in the CRE and the FRE are displayed in the left and right panels of Figure 7, respectively. We note that while the patterns are similar to those seen in Figure 6, the region of relatively large (r_h^{nd}) values off the coast of western Norway extends further south than the ensemble variances. Interestingly, we also find that CRE

and FRE patterns of r_h^{nd} are similar to each other, differing in magnitude by about a factor of 2. Hence, approximately half of the ratio of the FRE ensemble variances to the CRE variances ($\overline{\eta_{s,h;FRE}^2}^n / \overline{\eta_{s,h;CRE}^2}^n$) can be attributed to differences in the deterministic variability that results from refining the horizontal resolution ($\overline{\phi_{h;FRE}^2}^n / \overline{\phi_{h;CRE}^2}^n$), while the other half can be attributed to differences in the representation of flow instabilities due to the different resolutions in the FRE and the CRE ($r_{h;FRE}^{nd} / r_{h;CRE}^{nd}$).

In the present context, deterministic variability is associated with variability in the synoptic atmospheric forcing fields. Hence, we expect that for depth dependent quantities the fraction of nondeterministic variability is smallest near the surface. Differences in this fraction for salinity results at depths of 200 m and 10 m are displayed in Figure 8. Values are positive where the fraction of nondeterministic variability is largest for the 200 m salinities. Generally, Figure 8 shows that the fractions are largest for the 200 m salinities, as expected. This is the case in the entire Norwegian Trench, except for a very small band off the southern tip of Norway. How-

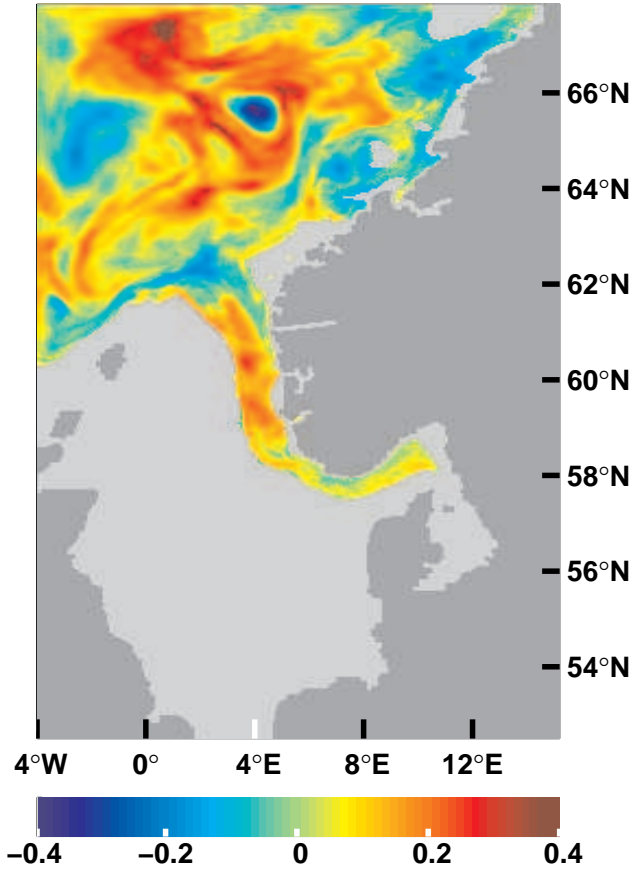


Fig. 8 Differences in fraction of nondeterministic variability in salinity (r_S^{nd}) from the FRE ensemble results, between depths of 200 m and 10 m. Values are positive where the fractions are largest at 200 m. The color coding of nondimensional fraction differences are displayed by the bar. Regions where the bottom depth is smaller than 200 m are light gray.

ever, in some regions elsewhere the fractions are largest for the 10 m salinities. One example of this is the steep continental slope in the Norwegian Sea (see Figure 1), where the circulation in the ocean’s interior is known to be heavily influenced by the presence of the slope (Skagseth et al. [20]).

6 Deterministic eddies and Skagerrak outbreak events

Outbreak events of water with low salinities from the Skagerrak into the North Sea occur episodically, mostly during fall and winter. Aure and Sætre [1] describe three such events that occurred in the severe winter of 1978 – 79. They suggest that such events take place after a period with westerly winds that have blocked the Skagerrak outflow. When the wind conditions change, a sudden outbreak of cold, low salinity water from the Skagerrak may take place. After such events, the intensity on the mesoscale is known to increase (Furnes et al. [9]). Thus, the possibility of “deterministic eddies” that was

hypothesized in the Introduction will be examined in the context of Skagerrak outbreak events.

In our examination of the model results we have identified a number of Skagerrak outbreak events. One example is presented in Figure 9a, where results for salinity from the fall of 1996 are shown in a Hovmöller diagram. These results were extracted from a band of model grid nodes about 20 km off the model coastline of southern Norway, from Lillesand in the south east to Bergen in the north west. An outbreak event from the Skagerrak can be seen to propagate along the coast from the Skagerrak and into the North Sea. The main part of the event occurs in mid November. (The freshwater anomalies that are seen in the east in October are terminated in the Skagerrak.) In the period 31 October – 10 November, there are very strong winds in the Skagerrak, initially from the southwest and later from the west. Then, the wind direction changes, and strong winds from the northeast dominate until 13 November.

In the aftermath of this event, two anticyclonic eddies can be observed in the model just to the west of the southern tip of Norway. The position of the eddies from three of the FRE ensemble members are indicated by a pair of arrows in Figure 9c–e. We observe that the results from the various members are very similar to each other. (Note that this is the case for all members, not just the three members that were chosen randomly to be displayed in Figure 9.) In order to quantify the differences in the ensemble results for the relative vorticity, the standard deviation for the full eight member ensemble was computed. The results in Figure 9b reveal that there are very small differences in relative vorticity for this date (23 November 1996).

Next, we revisit model results for relative vorticity on 25 September 2000 that were considered in section 5. As was the case for the fall of 1996, there is also a major outbreak of low salinity water in the fall of 2000. As can be seen from Figure 10a, this outbreak took place in early November. These are the model results for the event that was reported by Furnes et al. [9]. Based on sea level observations, they report that an outbreak event occurred during the first week of November 2000. The atmospheric forcing fields reveal that there were moderate to strong winds from the west in the Skagerrak during about 2.5 days starting 26 October. In the latter part of the period, the wind direction was from the southwest. The wind direction then reversed abruptly, and there were moderate to strong winds from the east until 30 October. Salinity data reviewed by Furnes et al. [9] display a drop of 1 – 1.5 PSU at Utsira (an island at about 59°N) during the first week of November. The corresponding drop in the model at this location is approximately 0.7 PSU.

However, the eddies in Figures 5 and 10c–e precede this event, and does not appear to be generated by an earlier event. The standard deviation of relative vorticity for the full eight member ensemble that is shown in

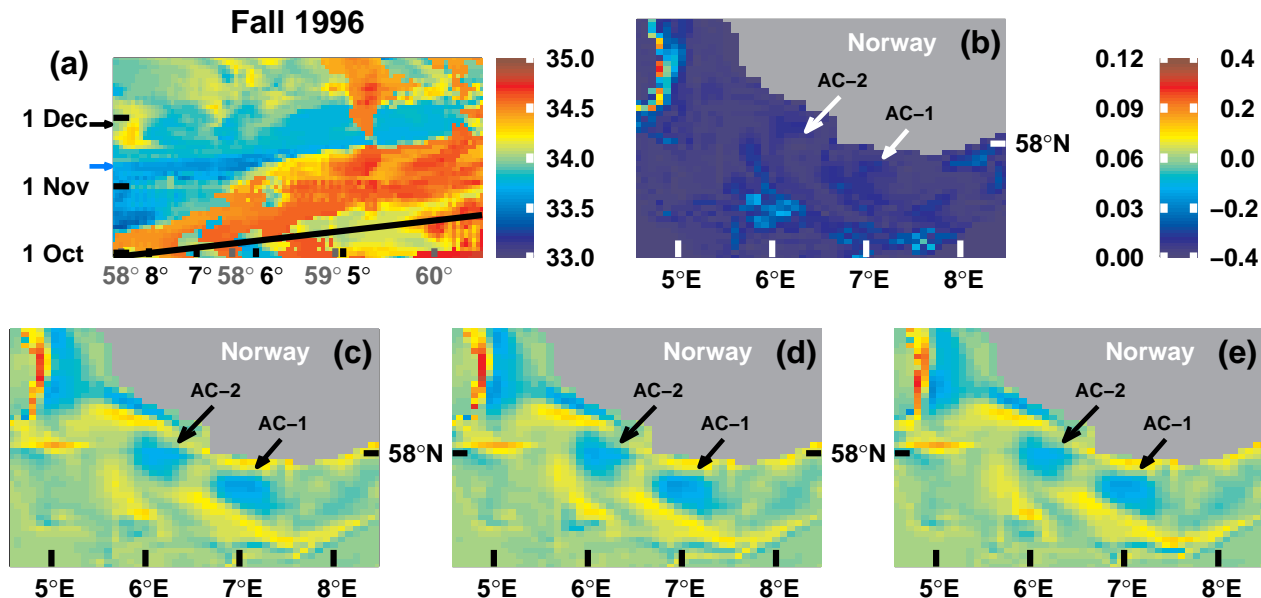


Fig. 9 A Skagerrak outflow event from the fall of 1996. (a): Hovmöller diagram for salinity along the southern coast of Norway, from Lillesand to Bergen (see black markers in Figure 1). FRE model results were extracted from a band approximately 20 km off the coast, at a depth of 30 m. Black and gray labels on the horizontal axis show longitudes and latitudes, respectively. The tilted line corresponds to a signal propagation speed of 0.30 m/s. The color coding is given by the bar to the right of panel (a), with values in PSU units. The blue arrow at the left vertical axis indicate the on-set of the main outbreak event, while the black arrow shows the date from which results are displayed in panels (b) – (e). (b): Standard deviation of relative vorticity for the full ensemble for 23 November 1996. (c) – (e): Model results for relative vorticity. Panels (c), (d), and (e) show results from FRE ensemble members *no.* 1, 4 and 7, respectively. These are the results for 23 November 1996. Arrows labeled AC-1 and AC-2 indicate the positions of two anticyclones. The arrows were placed in the same geographical positions in panels (b) – (e) for reference. The color coding used in panels (b) – (e) is displayed by the bar to the right of panel (b). Values to the left of the bar show the color coding in panel (b), while values to the right correspond to the coding in panels (c) – (e). Results in panels (b) – (e) have been scaled by the local Coriolis parameter.

Figure 10b displays remarkable differences from the 1996 event that was examined above: The standard deviations in this region, particularly in the North Sea, are much lower for the situation depicted in Figure 9b than is the case in Figure 10b. Moreover, while eddies AC-1 and C-1 in Figure 10c–e appear to be only modestly affected by the choice of initial conditions, AC-2 seem to be more affected by nondeterministic variability.

The tilted lines in Figures 9a and 10a correspond to a signal propagation speed of 0.30 m/s, as reported for this segment of the coast by Aure and Sætre [1] and Furnes et al. [9]. The propagation speed agrees well with our results.

An examination of the relative vorticity in the aftermath of the 2000 event reveals a presence of eddies that exhibit low fractions of nondeterministic variability in November, *i.e.*, in the aftermath of the outbreak event (not shown). Similar results were also found for a number of other outbreak events, *e.g.* in October – November 1998 and in December 1999.

7 Concluding remarks

We have investigated the ocean circulation in the Skagerrak and the North Sea by conducting two suites of ensemble simulations. The suites differed in the specification of the horizontal grid resolution, such that the coarser grid was constructed to be eddy permitting, while the finer grid simulations are close to being eddy resolving.

The model validation in section 3 revealed biases in the salinity and velocity fields consistent with a somewhat too wide coastal current. Nevertheless, mesoscale features are formed along the entire front of the NCC, when potential energy is converted to kinetic energy due to baroclinic instability. Hence, despite the biases, the present ensemble simulations are more than adequate for an examination of the role of flow instabilities on the variability of the ocean circulation in the North Sea.

In section 4 we found that the variability of the FRE ensemble may be slightly underestimated due to the possibility that the ensemble size is on the small side with respect to convergence. Nevertheless, the robustness of the results that were reported in sections 5 and 6 substantiate that our results are not critically sensitive to the present size of the ensemble.

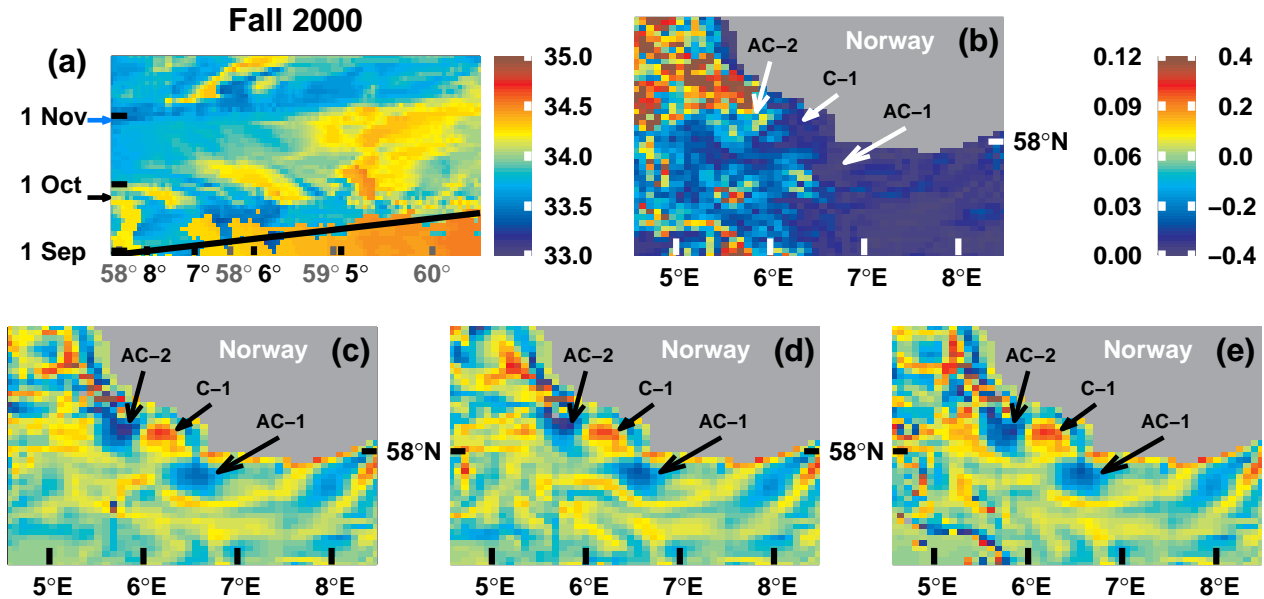


Fig. 10 Same as Figure 9, but for an event from the fall of 2000. Panels (b) – (e) show results for 25 September 2000. Panel (d) is the same as the left panel in Figure 5.

The first question posed in the Introduction was on the role of initial conditions and variability due to non-linear flow instabilities. This topic was investigated in section 5, where the variance of each of the ensembles were measured against the square offset of the ensemble mean from a climatology that was constructed based on the simulation results. We found that the ensemble variance is substantially affected by resolution, both in absolute terms and when measured against the total variance with respect to the climatology. The influence of flow instabilities, which increases as the model grid becomes finer and the resolved phenomena are more diverse, plays a significant role in this context. In the region under consideration, flow instabilities were found to have the largest impact on the ensemble variability in the frontal regions between the NCC and water masses of an Atlantic origin off the western and northwestern coast of southern Norway. In the southern North Sea and in the Skagerrak the variability among ensemble members was low, indicating that the actual variability in these regions is primarily due to the evolution of the synoptic atmospheric forcing.

The second question posed in the Introduction was if eddies that form on the front between the NCC and Atlantic Water can be deterministic. This topic was investigated in section 6, and our results show that even a feature that is formed by non-linear interactions may under certain conditions be described reliably without a perfect description of the initial conditions. This was seen to be the case for eddies to the west of the southern tip of Norway, particularly in the aftermath of Skagerrak outbreak events of low salinity water masses. Thus, in some cases eddies may be accurately described pro-

vided that the atmospheric forcing fields are known. We suggest that the wind history that leads to the Skagerrak outbreak events may be the agent that is responsible for these “deterministic eddies”, possibly in concert with vortex stretching and squeezing that take place when the flow traverses bottom topography features.

Acknowledgements I would like to thank E. Joseph Metzger (Navy Research Laboratory, Stennis, MS) for introducing me to the concept and interpretation of ensembles of model experiments. NCEP Reanalysis data were provided by the NOAA-CIRES Climate Diagnostics Center, Boulder, Colorado, USA, from their Web site at <http://www.cdc.noaa.gov/Hydrography> from the Hirtshals – Torungen transect was provided by the Institute of Marine Research in Norway. This study has been financed by the Norwegian Research Council under contract *no.* 146476/120. Computer time on a SGI Origin 3000 at the Norwegian high performance computing facility was granted by the Norwegian Research Council. Additional computations were performed at the Norwegian Meteorological Institute’s IBM Linux cluster. Thanks to Trond P. Bø at the institute for help to configure HYCOM at the cluster. Also thanks to Alan J. Wallcraft (Navy Research Laboratory, Stennis, MS) and Øyvind Sætra (Norwegian Meteorological Institute) for their valuable suggestions.

Appendix: Properties of ensemble variability

Since the ensemble members differ only in their initial states, differences in the results can be attributed to non-deterministic differences in both the initial conditions and the evolution of the simulations. A technique to separate variability of a prognostic variable into two components was suggested by Metzger and Hurlburt [18], and also used by Melsom et al. [17]. The technique was

recently refined by Melsom [16], and is repeated here for the sake of completeness.

Consider results for a prognostic variable η at a point in space, and define a partitioning of η by

$$\eta_s(n) = \tilde{\eta}_s(d_n) + \hat{\eta}(n) + \eta'_s(n) \quad (\text{A1})$$

where s is a member of ensemble simulations. Here, n is the time step, and d_n is the decimal day of time step n . $\tilde{\eta}_s(d_n)$ is the daily climatology for member s on day d_n . Further,

$$\hat{\eta}(n) = \frac{1}{S} \sum_{s=1}^S [\eta_s(n) - \tilde{\eta}_s(d_n)] \quad (\text{A2})$$

is the mean offset from the the daily climatologies. Then, from (A1) we see that η' is the departure of each member from the instantaneous ensemble mean as a function of space and time so that

$$\overline{\eta'_s(n)}^s = \sum_{s=1}^S \eta'_s(n) = 0 \quad (\text{A3})$$

where the overbar corresponds to an average over the ensemble members.

Using (A1) and (A3), the mean square offset from the daily climatology ($\tilde{\eta}_s$) may be expressed as

$$\phi^2 = \frac{1}{S} \sum_{s=1}^S [\eta_s - \tilde{\eta}_s]^2 = \hat{\eta}^2 + \overline{\eta'^2}^s \quad (\text{A4})$$

Here, the final term on the right hand side is the instant local variance of the ensemble members. The first term on the right hand side is the local square offset of the ensemble mean from the daily climatology.

Keeping in mind that $\hat{\eta}$ is independent of the variability from one member to another, the temporal mean of $\hat{\eta}^2/\phi^2$ is an estimate of the fraction of deterministic variability in response to atmospheric forcing. The non-deterministic variability fraction which is due to flow instabilities, is then given by

$$r^{nd} = \frac{\overline{\eta'^2}^s}{\phi^2} \quad (\text{A5})$$

Thus, r^{nd} enables us to quantify the contribution from nondeterministic variability as a fraction between 0 and 1 at each grid node. Note that the accuracy of this estimate depends on the size of the ensemble.

In the present study the daily climatology d_n was based on model results from November 1996 – October 2001, and a 30 day box filter was applied when the daily climatologies were computed. Decimal days were defined by numbering days from 1 January 1992 in cycles of 365.25 days.

Figure 11 displays the results for bSSH at a position in the eastern North Sea. The local daily climatology is given by the dashed line, the eight ensemble members are depicted by thin solid lines, and the ensemble mean is shown as the thick solid line. Then, the offset $\hat{\eta}$ of the

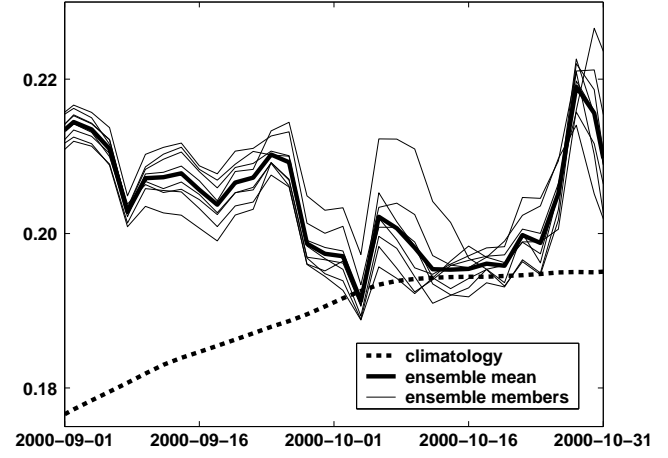


Fig. 11 Baroclinic sea surface height (in m) during September and October 2000. Results from the CRE are displayed for $3^\circ 50' E$, $61^\circ 42' N$, near the west coast of Norway. Thin lines correspond to the eight members, and the thick solid and dashed lines correspond to the ensemble mean values and the daily climatologies, respectively.

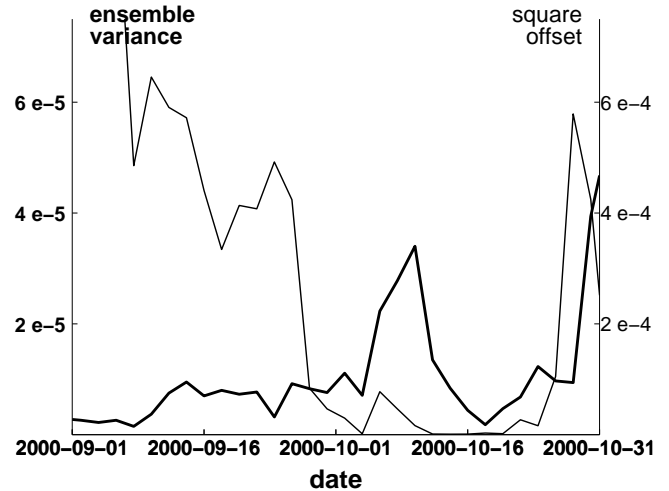


Fig. 12 The ensemble variance (thick line) and the square offset from the daily climatology (thin line), based on the results in Figure 11. Values along the vertical axes are in m^2 . Note that the resolution along the vertical axes differ by a factor of 10.

ensemble mean from the daily climatology is the distance from the dashed line to the thick solid line. The offset η'_s of ensemble member $no.$ s from the ensemble mean is the distance from the thick solid line to the thin line that displays the results from this member. The corresponding terms on the right hand side of Equation A4 are illustrated in Figure 12, where the ensemble variance and the square offset from the daily climatology are depicted as functions of time by the thick and thin lines, respectively.

References

1. Aure J, Sætre R (1981) Wind effects on the Skagerrak outflow. In: Sætre R Mork M (eds) The Norwegian Coastal Current. Proceedings Norwegian Coastal Current symposium, Geilo, 9-12 September 1980, Univ Bergen, Bergen, Norway, 263-293.
2. Bentsen M, Drange H, Furevik T, Zhou T (2004) Simulated variability of the Atlantic meridional overturning circulation. *Clim Dyn* 22 (6-7): 701-720 (doi: 10.1007/s00382-004-0397-x)
3. Bleck R (2002) An oceanic general circulation model framed in hybrid isopycnic-cartesian coordinates. *Ocean Model* 4: 55-88
4. Bleck R, Rooth C, Hu D, Smith LT (1992) Salinity thermocline transients in a wind- and thermohaline-forced isopycnic coordinate model of the Atlantic Ocean. *J Phys Oceanogr* 22: 1486-1505
5. Browning GL, Kreiss H-O (1982) Initialization of the shallow water equations with open boundaries by the bounded derivate method. *Tellus* 34: 334-351
6. Chassignet EP, Smith LT, Halliwell GR, Bleck R (2003) North Atlantic simulations with the HYbrid Coordinate Ocean Model (HYCOM): Impact of the vertical coordinate choice, reference pressure, and thermobaricity. *J Phys Oceanogr* 33: 2504-2526
7. Engedahl H, Eriksrød G, Ulstad C, Ådlandsvik B (1997) Climatological oceanographic archives covering the Nordic Seas and the Arctic Ocean with adjacent waters. Research report 59, Norw Met Inst, 69 pp
8. Engedahl H, Ådlandsvik B, Martinsen EA (1998) Production of monthly mean climatological archives for the Nordic Seas. *J Mar Syst* 14: 1-26
9. Furnes GK, Engedahl H, Hareide D, Aure J (2001) Ocean eddies along the coast of southern Norway: Looking back on the 18 November 2000 event at the Troll field. (In Norwegian, original title: Strømvirvler langs kysten av sør-Norge: Et tilbakeblikk på hendelsen ved Trollfeltet 18. november 2000.) Norsk Hydro Rep ID NH-00039406, Norsk Hydro Sandvika, Norway, 22 pp
10. Gammelsrød T, Hackett B (1981) The circulation of the Skagerrak determined by inverse methods. Sætre R Mork M (eds) The Norwegian Coastal Current. Proceedings Norwegian Coastal Current symposium, Geilo, 9-12 September 1980, Univ Bergen, Bergen, Norway, 311-330.
11. Halliwell GR (2004) Evaluation of vertical coordinate and vertical mixing algorithms in the HYbrid Coordinate Ocean Model (HYCOM). *Ocean Model* 7: 285-322
12. Hamill TM (2001) Interpretation of rank histograms for verifying ensemble forecasts. *Mon Weather Rev* 129: 550-560
13. Jerlov NG (1976) Marine Optics. Elsevier Oceanography Series. Elsevier Sci. Publ. Co., New York. 231 pp
14. Kalnay E, *et al.* (1996) The NCEP/NCAR 40-year reanalysis project. *Bull Am Meteor Soc* 77: 437-471
15. Large WG, McWilliams JC, Doney SC (1994) Oceanic vertical mixing: A review and a model with a nonlocal boundary layer parameterization. *Rev Geophys* 32: 363-403
16. Melsom A (2004) Nondeterministic variability in the Skagerrak and the North Sea: A pilot study. met.no report 11, Norw Met Inst, 19 pp (Available on-line at <http://ensemble.met.no/results/>)
17. Melsom A, Metzger EJ, Hurlburt HE (2003) Impact of remote oceanic forcing on Gulf of Alaska sea levels and mesoscale circulation. *J Geophys Res* 108: 3346 (doi: 10.1029/2002JC001742)
18. Metzger EJ, Hurlburt HE (2001) The nondeterministic nature of Kuroshio penetration and eddy shedding in the South China Sea. *J Phys Oceanogr* 31: 1712-1732
19. Røed LP, Fossum I (2004) Mean and eddy motion in the Skagerrak/northern North Sea: insight from a numerical model. *Ocean Dyn* 54: 197-220
20. Skagseth Ø, Orvik KA, Furevik T (2004) Coherent variability of the Norwegian Atlantic Slope Current derived from TOPEX/ERS altimeter data. *Geophys Res Lett* 31: L14304 (doi: 10.1029/2004GL020057)
21. Sætre R (1983) Ocean currents in the upper layers off Norway. (In Norwegian, original title: Strømforholdene i øvre vannlag utenfor Norge.) Rep. no. FO 8306, Inst. of Mar. Res., Bergen, Norway.